Journal of Biomedical Optics

SPIEDigitalLibrary.org/jbo

Comparison of Schlemm's canal's biological parameters in primary open-angle glaucoma and normal human eyes with swept source optical

Fei Wang
Guohua Shi
Xiqi Li
Jing Lu
Zhihua Ding
Xinghuai Sun
Chunhui Jiang
Yudong Zhang

SPIE

Comparison of Schlemm's canal's biological parameters in primary open-angle glaucoma and normal human eyes with swept source optical

Fei Wang,[c*] Guohua Shi,[a,b*] Xiqi Li,[a,b] Jing Lu,[a,b] Zhihua Ding,[d] Xinghuai Sun,[c] Chunhui Jiang,[c] and Yudong Zhang[a,b]
[a]Chinese Academy of Sciences, The Key Laboratory on Adaptive Optics, Chengdu 610209, China
[b]Institute of Optics and Electronic, Chinese Academy of Sciences, Chengdu 610209, China
[c]Fudan University, Department of Ophthalmology and Vision Science, Eye & ENT, Shanghai 200031, China
[d]Zhejiang University, State Key Laboratory of Modern Optical Instrumentation, Hangzhou 310027, China

Abstract. Thirty-seven normal and primary open angle glaucoma (POAG) subjects were noninvasively imaged by a tailor-made real-time anterior segment swept source optical coherence tomography (SS-OCT) to demonstrate the differences of the Schlemm's canal (SC) between POAG and normal eyes. After the cross-section images of the anterior chamber angle were acquired by SS-OCT, SC was confirmed by two independent masked observers and the average area, long diameter, and perimeter of the SC were measured. In normal subjects the circumference, area, and long diameter is 580.34 ± 87.81 μm, 8023.89 ± 1486.10 μm^2, and 272.83 ± 49.39 μm, respectively, and these parameters were 393.25 ± 98.04 μm, 3941.50 ± 1210.69 μm^2, and 190.91 ± 46.47 μm in the POAG subjects. The area of SC in the normal ones was significantly larger than that in POAG eyes ($p < 0.001$), so as the long diameter and the perimeter ($p < 0.001$; $p < 0.001$).
[DOI: 10.1117/1.JBO.17.11.116008]

Keywords: optical coherence tomography; ophthalmology; Schlemm's canal; morphometry; glaucoma.

Paper 12399 received Jun. 26, 2012; revised manuscript received Sep. 21, 2012; accepted for publication Oct. 2, 2012; published online Nov. 1, 2012.

1 Introduction

Glaucoma is a group of progressive optic neuropathies and now is the second leading cause of blindness worldwide.[1] It is estimated that more than 66 million individuals suffered from the disease with at least 6.8 million bilaterally irreversibly blind.[2] Though the pathogenesis of glaucoma is not yet fully understood, intraocular pressure (IOP) is the only proven treatable risk factor.[3,4] Abnormally high IOP is a risk factor related to the death of retinal ganglion cells and optic nerve fibers, resulting in a distinct appearance of the optic disk and a concomitant pattern of visual loss in almost all glaucoma patients.[5]

IOP is regulated by a balance between the secretion and drainage of the aqueous. After being secreted by the ciliary body, the fluid mainly pours out the eye via the trabecular meshwork draining into Schlemm's canal (SC) and then to the collector channels (CC) which finally empty into the venous circulation.[6]

For the sake of a better study of the pathophysiology and other aspects of glaucoma, imaging of the aqueous pathway is important. The resistance points of aqueous humor outflow in primary open-angle glaucomatous eyes is located in a trabecular meshwork and (or) structures downstream of it.[7] The Schlemm's canal, which connects the trabecular meshwork and collector canals, alone might explain approximately 50% of the decreased aqueous outflow facility in these patients.[7] In 1970, Nesterov speculated that the collapse of SC at higher IOP might be a cause of primary open-angle glaucoma.[8] Studies in cadaver eyes suggested that glaucomatous eyes have smaller SCs than those of healthy individuals.[9] A recent study suggested that Schlemm's canal becomes wide at low IOPs and collapses when the IOP is increased. This collapse might cause extra blockage on the outflow of the aqueous then form a vicious circle.[10] These findings, however, were speculated from cadaver studies, so what happens in normal or glaucomatous eyes has not been fully understood.

In vivo observation of SC would give us more information. Slit-lamp microscopes and ultrasound biomicroscopes (UMB) are being used for the observation of the structures.[11] Slit-lamp microscopes, however, cannot provide a cross-sectional image. The UMB test has to contact the eyes, which carries a risk of infection.[12] The extra extension over the eye added by the washing cup and eyelid retractor in the UBM may also subtly influence the measurement.[13] A noninvasive, *in vivo* way to study the SC in the human eye was required to improve our understanding of the SC.

Optical coherence tomography (OCT) has been applied to reveal the anterior segment of the eye.[14,15,16] Kagemann et al. tried, however, several deficiencies still exist.[17] First, the SC is located behind the sclerocorneal junction, so a light source of high penetrating ability was required.[12] However, the 870 nm light source they used could not provide high penetration and signal-to-noise ratio (SNR) for anterior segment imaging. What's more, there were only three glaucoma patients in their study and only one of the patient's SC was successfully imaged. We have used a tailor-made 1310 nm swept source optical coherence tomography (SS-OCT). Compared to 870 nm SD-OCT, the 1310 nm SS-OCT has better SNR and penetration. Moreover, SCs' morphometric values of 50 normal people were

*Guohua Shi and Fei Wang contributed equally to this work.

Address all correspondence to: Guohua Shi, Chinese Academy of Sciences, The Key Laboratory on Adaptive Optics, Chengdu 610209, China. Tel: 0086-28-8510-0630; E-mail: guohua_shi@yahoo.com.cn.

0091-3286/2012/$25.00 © 2012 SPIE

assessed successfully in our previous research.[18] In order to further demonstrate the differences of SC between glaucomatous and normal eyes, we implemented the following study.

The main works of this paper are listed as follows. Section 1: swept source OCT with 1310 nm light source were used in our research in order to acquire clear and high resolution images. Moreover, real-time signal processing was used in this study, making it more convenient for testing and observation. Section 2: 18 primary open angle glaucoma (POAG) patients and 19 sex- and age-matched controls were enrolled and the biological parameters of SC were measured. Section 3: the biological parameters of SC in the two groups were compared. With these three sections, the recent research aims to explore the differences more objectively and comprehensively.

2 Methods

2.1 *Anterior Segment OCT System*

The tailor-made anterior segment OCT system applied in our study is shown in Fig. 1. The light source is a swept-source laser (HSL-2000, Santec, Japan) with a 1310 nm center wavelength and a 110 nm scan range. A Michelson-type OCT interferometer (INT-MSI-1300, Thorlabs) with a dual-balance detector is applied to detect the interference data. Then a Mach-Zehnder interferometer (INT-MZI-1300, Thorlabs) is used to calibrate the wavelength. The interference and calibration data were obtained by a two-channel data acquisition card (NI 5122. 100 Ms/s, National Instrument). A waveform generation card (NI 6221, National Instrument) generates the waveform to drive the galvo mirror and trigger the data acquisition card for each A-scan. Real-time signal processing was realized by the graphics processing unit (GPU).[19] The B-scan image contains 800 A-lines, and its frame rate is 20 frames per second. The axial resolution is 8.03 μm in air and 6 μm in tissue approximately by considering the reflective index of aqueous is 1.34 (Ref. 20).

The morphometric measurement of SC is incident beam angle dependent. So a special mechanism is taken into the system to reduce the motion artifact. Figure 1(b) and 1(c) shows the details. As is shown in Fig. 1(b), the Michelson interferometer, Mach-Zehnder interferometer, and reference arm are fitted in a motherboard. The sample arm is connected to a three-dimensional electric translation stage which is manually controlled by six buttons on the front control panel to adjust the imaging location and focusing position. The gantry structure allows the subject to lie down, and makes the subject more

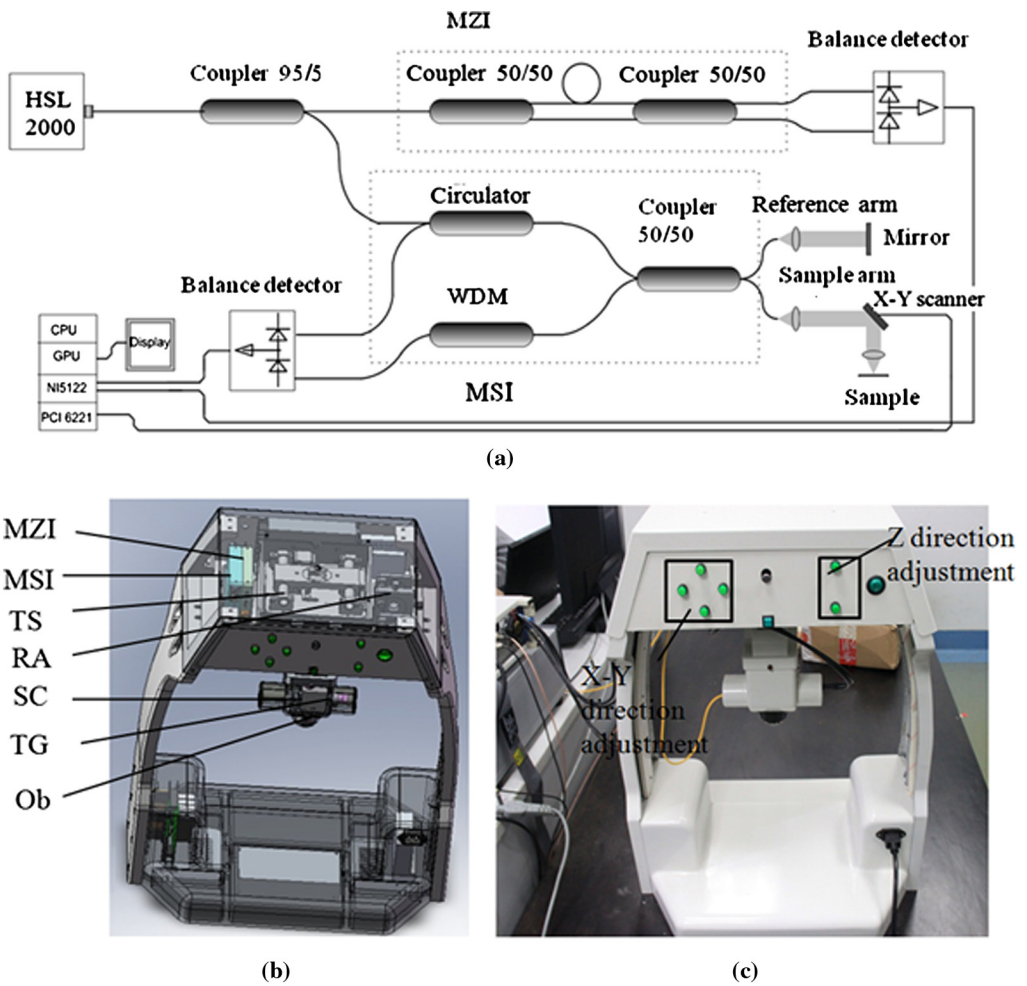

Fig. 1 (a) Schematic of the SS-OCT system. (b) Structure diagram of the SS-OCT system. (c) The picture of the SS-OCT system. WDM: wavelength division multiplexer; SC: *x-y* scanner; Ob: objective; MZI: Mach-Zehnder interferometer; MSI: Michelson interferometer; RA: reference arm; SA: sample arm; TS: 3-dimensional electric translation stage; and TG: target.

comfortable, which leads to reduced eye motion and ensures different subjects in roughly the same incidence beam angle.

The subjects take the recumbent posture when they are examined. One operator completes all the operations including locating, focusing, imaging, and recording. The system was calibrated, and the image was extended to be the approaching resolution in axial and lateral directions.

Figure 2(a) shows the SS-OCT image of the anterior segment in a normal human eye and the inserts are enlarged images taken from the original image. When we carry out the morphometric measurement, we zoom in on the image and use a polygon to draw the profile of SC manually. As is shown in Fig. 2(a), the SC appears as a dark slit, oval, or triangular-like structure locating anterior to the outer 2/3 part of the trabecular meshwork. The SC area, perimeter, and the longest diameter was defined as the area, perimeter, and the longest diameter of the white slit-like structure. So the diameter can be obtained by the farthest distance of the two pixels, the perimeter can be obtained by the sum of distances, and the area can be obtained by the polygonal area formula as Eq. (1) shows.

$$S_\Omega = \frac{1}{2}\sum_{i=1}^{M}(x_i \times y_{i+1} - x_{i+1} \times y_i)d_x d_y, \tag{1}$$

where x_i and y_i are the pixels' coordinates, and d_x and d_y are the lengths that each pixel represents in the transverse and axial directions, respectively. When the cross-section image consists of 800 A-lines, the transverse scan range is 4.8 mm in air, so each pixel represents 6 μm length in transverse. Each A-line contains 512 pixels, so the axial scan range is 2.97 mm in air. So by considering the refractive index of the aqueous, each pixel represents 4.3 μm in axial length when the pixel is in the aqueous.

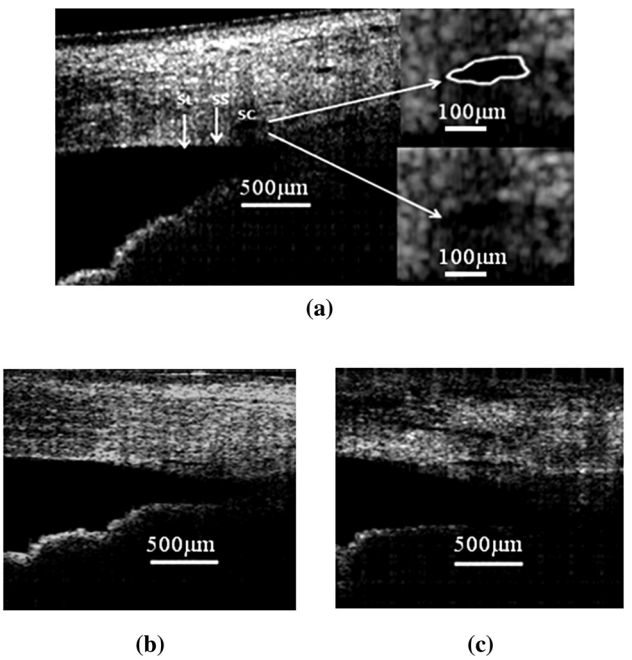

Fig. 2 (a) The SS-OCT anterior segment image of the 36th normal subject. (b) The SS-OCT anterior segment image of the 55th POAG patient. (c) The SS-OCT anterior segment image of the 40th normal subject. SS: sclera spur; SL: Schwalbe line; and SC: Schlemm's canal.

Figure 1(b) and 1(c) are images of a 26-year-old female patient who was diagnosed with POAG and a 45-year-old normal female subject, respectively. The morphological differences of the SC between glauconous and normal eyes can be observed intuitional from the images clearly, and detailed analysis is made in Sec. 3.

3 Experiment

3.1 *Subjects*

The study was conducted in accordance to the tenets of the declaration of Helsinki. The ethics committee of the Eye, Ear, Nose, and Throat Hospital, Fudan University approved the study. All subjects were recruited from patients who visited the Eye, Ear, Nose, and Throat Hospital. Each patient underwent a complete ophthalmic examination including: a review of relevant medical history, best corrected visual acuity (BCVA), noncontact lens slit-lamp biomicroscopy (Volk Super Field® USA), anterior segment angle exam (Volk G-1 trabeculum® USA), (IOP, Goldman T900, HAAG-STREIT Schweiz), and visual field examination (VF, Humphrey Field Analyzer; Humphrey Matrix Frequency Doubling Technology Perimeter; Carl Zeiss Meditec, Dublin, California). All the normal participants were checked using a frequency doubling technology perimeter (FDT) and the glaucomatous ones by the Humphrey Field Analyzer.

The criteria for normal subjects are BCVA 20/25 or better, an IOP 21 mm Hg or less, normal fundus, including an intact rim, no evidence of hemorrhage, notching, excavation, and asymmetrical optic disks (asymmetry of vertical cup-disk ratio >0.2), normal VF results, a negative family history of glaucoma, and a negative history of ophthalmic disease and surgery. The including criteria for POAG patients are an IOP $\geq$ 21 mmHg, a typical glaucoma optic neuropathy (dish rim narrow or loss, nerve fiber layer defect, optic disk bleeding), visual field abnormality correspondence to optic nerve change, and the anterior segment angle open. Patients who have signs of congenital or secondary glaucoma, optic neuropathy other than glaucoma, or a history of ocular surgery were not included. Patients with optic media opacity such as corneal diseases, severe cataract, vitreous body cloudy, etc. were also excluded.

Participants were examined in the supine position by a single examiner. An external light dot was used to help fixation during the exam. The anterior segment angle scan protocol was used for scanning the angle at the 3 and 9 o'clock positions, respectively, and each image contained 800 A-lines. Each position was imaged twice and the images were stored for further analysis. Another single examiner reviewed all the images and chose the clear one for further analysis and measurements.

In order to get statistical results, SPSS13.0 (SPSS, Inc, Chicago, Illinois, USA) was used to discern the differences of the parameters between normal eyes and POAG ones. A p value less than 0.05 was considered statistically significant. The entire statistics test adopts a two-tailed test. After the Shapiro-Wilk test, the normal distribution material was described as mean $\pm$ SD and the median was used for nonnormal distribution material (25 and 75 percent percentile Interquartile, IQR).

4 Results

Thirty-seven participants were involved in the study: 19 in the normal group including 12 men (63%) and 7 (37%) women, aged from 20 to 74 years old (53.32 $\pm$ 18.32); and 18 in the

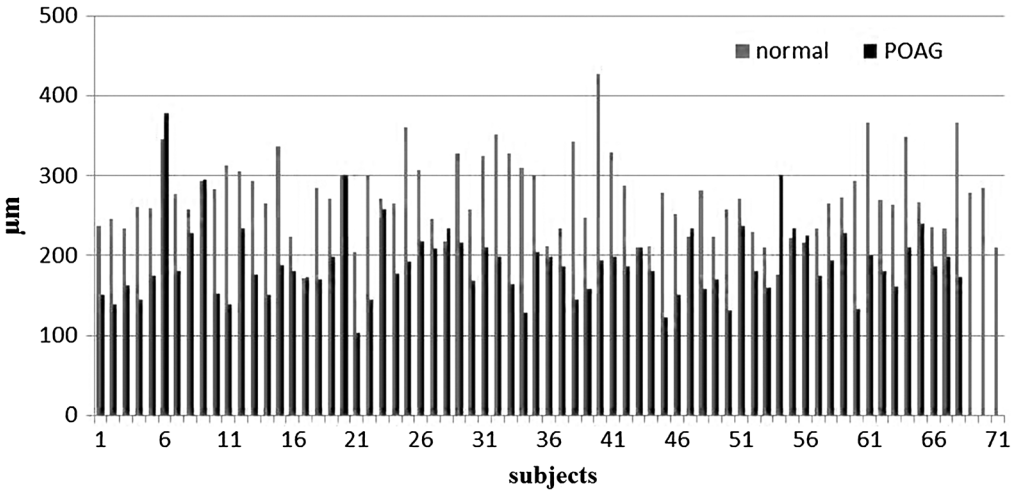

(a)

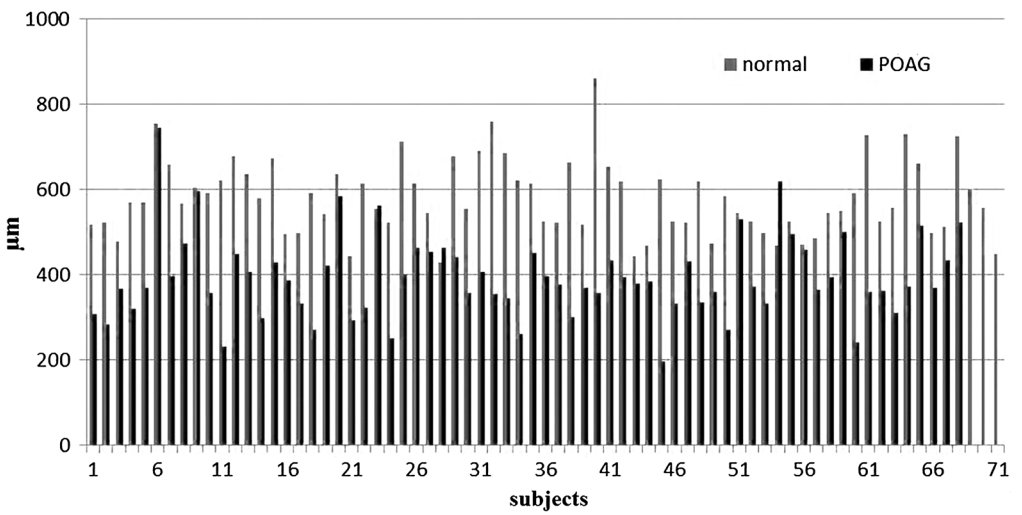

(b)

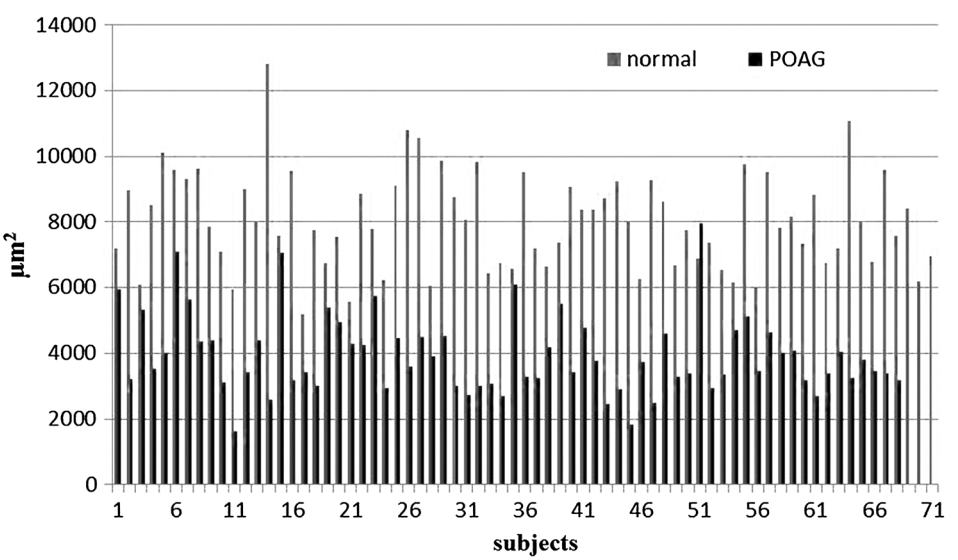

(c)

Fig. 3 The biological parameters of SC in normal and POAG subjects: (a) is the distribution of the long diameter; (b) is the distribution of the perimeter; and (c) is the distribution of the area.

POAG group including 8 men (44%) and 10 (56%) women, aged from 19 to 76 years old (49.61 ± 18.58). All 18 patients in the glaucoma group were bilateral.

There is no significant difference in the distribution of age ($p = 0.55$) and gender ($p = 0.25$) between the primary open-angle glaucoma and normal control group in our study. The IOP of POAG group (21 to 29, average 23.53 ± 2.30 mmHg) is higher ($p < 0.001$) than that of the control ones (12 to 19, 12.53 ± 1.81 mmHg).

The cross-section images of the anterior chamber angle were captured in all 74 eyes, including important structures like cornea, iris, scleral spur, trabecular meshwork, and Schlemm's canal. The SC can be discerned in 142 of the 148 scans (95.9%). Six eyes' SCs cannot be imaged successfully, including 2 normal and 4 glaucomatous eyes. SCs' morphometric values were measured and described as oculus dexter nasal (ODN), oculus dexter temporal (ODT), oculus sinister nasal (OSN), and oculus sinister temporal (OST), respectively, and all morphometric values are shown in Fig. 3. The statistical results of SC morphometric values are shown in Table 1.

Table 1 The statistical values in include the perimeter, area, and long diameter of the SC in normal and POAG eyes. The word "average" means the average value of the perimeter, area, and long diameter of the OD and OS including the temperial and the nasal sides. The sample number of the "average" is 74 and 68 in normal and POAG group, respectively. These parameters are larger in the normal group and the differences between the two groups were statistically significant. By analyzing the statistical values, there was no difference in the success rate of Schlemm's canal imaging between the normal and the POAG group ($p = 0.49$), or the nasal and temporal in both the normal group ($p = 0.49$) and POAG ($p = 1.00$). The perimeter, area, and long diameter of the Schlemm's canal from the nasal and temporal were alike in both the normal (perimeter $p = 0.81$; area $p = 0.91$; and long diameter $p = 0.34$) and the POAG group (perimeter $p = 0.16$; area $p = 0.96$; and long diameter $p = 0.20$). But a statistically significant difference between the normal and POAG group was noted with all being less in the POAG eyes (shown in Fig. 2, Table 1).

5 Discussion

This study indicated that swept-source OCT can be used in high-resolution imaging of the anterior chamber angle including important fine structure such as Schlemm's canal. Meanwhile, biological parameters of Schlemm's canal can be accessed properly.

This time, important structures, such as the cornea, iris, scleral spur, and trabecular meshwork of the anterior segment

Table 1 The morphometric values of SC in normal and POAG subjects.

		SC perimeter (mean ± standard deviation)	SC cross section area (mean ± standard deviation)	SC long diameter (mean ± standard deviation)
Normal	ODN	589.31 ± 73.00	8340.00 ± 1791.96	271.67 ± 41.97
	ODT	593.15 ± 88.89	8012.21 ± 1620.65	283.66 ± 46.62
	OSN	565.49 ± 102.54	7728.00 ± 1074.29	262.45 ± 61.08
	OST	571.39 ± 89.80	7998.12 ± 1391.12	272.32 ± 48.66
	OD	591.28 ± 80.45	8171.68 ± 1690.32	277.83 ± 44.22
	OS	568.44 ± 94.96	7863.06 ± 1231.52	267.38 ± 54.61
	Nasal	577.74 ± 88.09	8042.74 ± 1498.32	267.19 ± 51.56
	Temporal	582.87 ± 88.72	8005.56 ± 1495.15	278.30 ± 47.26
	Average	580.34 ± 87.81	8023.89 ± 1486.10	272.83 ± 49.39
POAG	ODN	390.26 ± 122.82	4182.33 ± 1508.28	189.77 ± 61.41
	ODT	398.96 ± 96.61	3947.25 ± 969.05	195.14 ± 48.66
	OSN	360.96 ± 64.44	3686.50 ± 1127.50	176.89 ± 30.62
	OST	419.89 ± 95.53	3922.22 ± 1195.24	200.76 ± 39.00
	OD	394.36 ± 109.69	4071.71 ± 1270.02	192.30 ± 55.01
	OS	392.16 ± 86.49	3811.29 ± 1152.41	189.53 ± 36.82
	Nasal	376.48 ± 99.39	3949.00 ± 1346.43	183.71 ± 49.11
	Temporal	410.04 ± 95.16	3934.00 ± 1078.40	198.11 ± 43.22
	Average	393.25 ± 98.04	3941.50 ± 1210.69	190.91 ± 46.47
p value		$p < 0.001$	$p < 0.001$	$p < 0.001$

angle were successfully imaged in all subjects of the anterior segment angle and the SCs could be determined in 95.9% of them. The location and shape of SC in our study coincide with the histological result.[21] This high success rate might be contributed to several reasons. Firstly, the system adopts a light source of 1310 nm, which has a better penetration and SNR than the 870 nm one for the image of the anterior segment of human eye. Consequently, high-quality images can be obtained. Secondly, a horizontal mechanical structure was introduced to the system, where patients can be examined just laying in bed, and thereby reducing the influence of body shaking during the examination. This design not only increases the "comfort level" to improve the patients' cooperation, allowing the old POAGs to keep the eye position steady during imaging, but also gives the operators more time to search SC, so as to increase the success rate of the imaging. Besides, we have carefully calibrated the axial and transverse scan ranges at first, which eliminates the measurement error caused by the refractive index. Finally, the system can realize video-level data acquisition, data processing, and display by using a GPU. The real-time observations of the anterior segment of the eyes came true. Operators can observe the sectional structure easily. There are still six positions from six eyes, in which SC can not be distinguished clearly. The first might be the age. Previous research indicated that the sclera become thicker with the ageing process. Moreover, the sclera is thickest at corneoscleral limbus, where SC is located. This might reduce the penetration of scanning light in elder subjects. Two undiscerning SCs are from eyes of the oldest two subjects in the normal group (71 and 74 years old), though there is no significant statistical difference between the ages of these two subject and other normal (Mann-Whitney U Test $u = -1.37$, $p = 0.21$). The other reason might be the pathological damage of POAG. The SCs might have collapsed due to the prolonged elevation of IOP. Histological research indicated that the collapsing of SC in POAG eyes is not uncommon. Also in the histo-study, it was found that the SC in some POAG eyes was difficult to discern.[7] So, we deduced the absence of the SC on the OCT image might be the result of the collapsing of SC.

The age and gender in the study are consistent with the clinical characteristics of POAG.[22] At the same time, the biological parameters of Schlemm's canal were successfully measured. Previously, measurements were histologically made. OCT increases the accuracy as well as the reliability in a noncontact way. In the early SD-OCT study, a hyporeflective band at the interface of the trabecular meshwork was taken as the Schlemm's canal, but the big difference was noted between theirs and the pathological results.[23] Recently Kagemann et al. reported imaging of Schlemm's canal by Fourier domain OCT, which was further verified by Doppler signal. Ours and their results are alike, and are both similar to the pathologic ones.[17]

It is further found that the area, perimeter, and long diameter of Schlemm's canal in POAG patients were smaller than those in the control ones. These results were in good agreement with the previous pathological studies.[7] The reason for the difference between normal and glaucomatous eye is not well understood. The prolonged elevated IOP pressing against the SC might be one of the reasons. But since the structure at the limbus is sophisticated, different tissue might change differently under the pressure. The pathological change of the surrounding tissue might cause extra or second force from different directions. So the SC might not only change in the direction of the IOP pressing, but also in others as well. These may contribute to the shortening of the long diameter in POAG eyes. Meanwhile, this study included more glaucomatous eyes, which made the result more reliable and significative than previous research. Despite many years of dedication to the nosogenesis of POAG, it is still unknown until now and there is dispute about the exact block point of POAG. The smaller SC perimeters in POAGs might reflect the difficulty of aqueous drainage in these patients and clue the block point finding. The noninvasive method and the results of our research might provide another way and perspective in the pathogenesis research, which may help in searching for effective and suitable methods to conquer the disease. Regarding the assessment of curative effect of medicine or surgery, objectively gauging the SCs might represent the drainage of the aqueous to some extent.

On the other hand, our study was still limited by its small number of participants. And we only got two images for each subject, one from the nasal and the other one from the temporal side. It is generally accepted that great variation exists in different parts of the Schlemm's canal, so future work with a comprehensive 360 deg imaging of the SC is required to present the overall situation.[24]

6 Conclusions

In conclusion, SC can be noninvasively imaged and measured in the living human eye by swept source OCT, and the morphometric measurement of normal and POAG's SC was made successfully. This might be useful in evaluating the facility of aqueous outflow to some extent and used clinically to study the mechanism of anti-glaucoma medications, as well as the effectiveness of surgical treatment by observing and/or comparing the SC. In the future, we will extend the sample to analyze the correlation between the age, IOP, and SC morphometric values in normal and POAG human eyes, and make a detailed comparison of SC morphometric values between different medicated patients in POAG human eyes to study the medical efficacy of anti-glaucoma medications.

Acknowledgments

This research was supported by the National Science Foundation of China (Grant No. 61108082), the Knowledge Innovation Program of the Chinese Academy of Sciences (Grant No. KGCX2-Y11-920), and the Research Foundation of Fudan University (Grant No. JJF158005).

References

1. R. N. Weinreb and P. T. Khaw, "Primary open-angle glaucoma," *Lancet* **363**(9422), 1711–1720 (2004).
2. H. A. Quigley, "Number of people with glaucoma worldwide," *Br. J. Ophthalmol.* **80**(5), 389–393 (1996).
3. A. Sommer et al., "Relationship between intraocular pressure and primary open angle glaucoma among white and black Americans. The Baltimore Eye Survey," *Arch. Ophthalmol.* **109**(8), 1090–1095 (1991).
4. I. O. Haefliger, "Risk factors associated with glaucoma," *Klin. Monbl. Augenheilkd.* **210**(5), 265–268 (1997).
5. A. J. Bellezza et al., "Deformation of the lamina cribrosa and anterior scleral canal wall in early experimental glaucoma," *Invest. Ophthalmol. Vis. Sci.* **44**(2), 623–637 (2003).
6. W. M. Grant, "Clinical measurements of aqueous outflow," *Am. J. Ophthalmol.* **34**(11), 1603–1605 (1951).
7. R. R. Allingham, A. W. de Kater, and C. R. Ethier, "Schlemm's canal and primary open angle glaucoma: correlation between Schlemm's canal dimensions and outflow facility," *Exp. Eye Res.* **62**(1), 101–109 (1996).

8. A. P. Nesterov, "Role of the blockade of Schlemm's canal in pathogenesis of primary open-angle glaucoma," *Am. J. Ophthalmol.* **70**(5), 691–696 (1970).
9. E. Lutjen-Drecoll et al., "Quantitative analysis of 'plaque material' in the inner- and outer wall of Schlemm's canal in normal- and glaucomatous eyes," *Exp. Eye Res.* **42**(5), 443–455 (1986).
10. R. D. Ten Hulzen and D. H. Johnson, "Effect of fixation pressure on juxtacanalicular tissue and Schlemm's canal," *Invest. Ophthalmol. Vis. Sci.* **37**(1), 114–124 (1996).
11. C. J. Pavlin, M. D. Sherar, and F. S. Foster, "Subsurface ultrasound microscopic imaging of the intact eye," *Ophthalmol.* **97**(2), 244–250 (1990).
12. S. Radhakrishnan et al., "Comparison of optical coherence tomography and ultrasound biomicroscopy for detection of narrow anterior chamber angles," *Arch. Ophthalmol.* **123**(8), 1053–1059 (2005).
13. T. Dada et al., "Comparison of anterior segment optical coherence tomography and ultrasound biomicroscopy for assessment of the anterior segment," *J. Cataract Refract. Surg.* **33**(5), 837–840 (2007).
14. S. Asrani et al., "Detailed visualization of the anterior segment using Fourier-Domain optical coherence tomography," *Arch. Ophthalmol.* **126**(6), 765–711 (2008).
15. Y. Yasuno et al., "Three-dimensional and high-speed swept-source optical coherence tomography for *in vivo* investigation of human anterior eye segments," *Opt. Express* **13**(26), 10652–10664 (2005).
16. Y. Yasuno et al., "Visibility of trabecular meshwork by standard and polarization sensitive optical coherence tomography," *J. Biomed. Opt.* **15**(6), 061705 (2010).
17. L. Kagemann et al., "Identification and assessment of Schlemm's canal by spectral-domain optical coherence tomography," *Invest. Ophthalmol. Vis. Sci.* **51**(8), 4054–4059.
18. G. Shi et al., "Morphometric measurement of Schlemm's canal in normal human eye using anterior segment swept source optical coherence tomography," *J. Biomed. Opt.* **17**(1), 016016 (2012).
19. X. Li et al., "High-speed optical coherence tomography signal processing on GPU," *J. Phys.: Conf. Ser.* **277**(1), 12–19 (2011).
20. T. Olsen, "On the calculation of power from curvature of the cornea," *Br. J. Ophthalmol.* **70**(2), 152–154 (1986).
21. W. H. Spencer, J. Alvarado, and T. L. Hayes, "Scanning electron microscopy of human ocular tissues: trabecular meshwork," *Invest. Ophthalmol.* **7**(6), 651–662 (1968).
22. A. R. Rudnicka et al., "Variations in primary open-angle glaucoma prevalence by age, gender, and race: a Bayesian meta-analysis," *Invest. Ophthalmol. Vis. Sci.* **47**(10), 4254–4261 (2006).
23. M. V. Sarunic, S. Asrani, and J. A. Izatt, "Imaging the ocular anterior segment with real-time, full-range Fourier-domain optical coherence tomography," *Arch. Ophthalmol.* **126**(4), 537–542 (2008).
24. C. Buller and D. Johnson, "Segmental variability of the trabecular meshwork in normal and glaucomatous eyes," *Invest. Ophthalmol. Vis. Sci.* **35**(11), 3841–3851 (1994).